Eur. Phys. J. Plus (2021) 136:499
https://doi.org/10.1140/epjp/s13360-021-01486-w

THE EUROPEAN PHYSICAL JOURNAL PLUS

Regular Article

Double-diffusive Air-CO_2 mixture flow in a staggered cavity with numerous concave lower wall aspect ratios

Hassanein I. Khalaf[1,a], **Khalid B. Saleem**[1,b], **Khaled Al-Farhany**[2,c], **Wael Al-Kouz**[3,d]

[1] Mechanical Engineering Department, Engineering College, University of Basrah, Basrah, Iraq
[2] Department of Mechanical Engineering, University of Al-Qadisiyah, Al-Qadisiyah, Iraq
[3] Department of Mechanical and Maintenance Engineering, School of Applied Technical Sciences, German Jordanian University, Amman 11180, Jordan

Received: 8 March 2021 / Accepted: 23 April 2021

Abstract In this paper, double-diffusion natural convection for staggered cavities with a concaved lower wall is investigated. The finite volume procedure is utilized to solve the governing equations along with the boundary conditions. The current code is validated with previously published results. Impacts of Rayleigh number ($10^4 \leq \mathrm{Ra} \leq 10^6$), buoyancy ratio ($-5 \leq N \leq 5$), Lewis number ($1 \leq \mathrm{Le} \leq 5$), and aspect ratio ($0.1 \leq \mathrm{AR} \leq 0.2$) on the flow characteristics are investigated and presented as isotherms, streamlines, and iso-concentrations contours. Moreover, alterations of average Nusselt and average Sherwood numbers with these parameters are analyzed and discussed thoroughly. It is found that average Nusselt and average Sherwood numbers augment with Rayleigh number and buoyancy ratio for aiding flows. These also are found to decrease with decreasing buoyancy ratio for opposing flows. Also, it is elucidated that the aspect ratio has an inverse relationship with average Nusselt and average Sherwood numbers in which the depression in these numbers is determined to be 10.4%.

List of symbols

AR	Aspect ratio
c	Concentration (kg m^{-3})
C	Dimensionless concentrations
D	Mass diffusivity (m^2 s^{-1})
g	Gravity acceleration (m s^{-2})
L	Cavity length (m)
Le	Lewis number
N	Buoyancy ratio

[a] e-mail: hassanein.khalaf@uobasrah.edu.iq
[b] e-mail: khalid.saleem@uobasrah.edu.iq (corresponding author)
[c] e-mail: khaled.alfarhany@qu.edu.iq
[d] e-mail: wael.alkouz@gju.edu.jo

Published online: 06 May 2021

Nu_{avg}	Average Nusselt number
p	Pressure (Pa)
P	Dimensionless pressure
Pr	Prandtl number
R	Arc radius (m)
Ra	Rayleigh number
Sh_{avg}	Average Sherwood number
T	Temperature (K)
u,v	Velocity components (m s^{-1})
U, V	Dimensionless velocity components
x,y	Dimensional coordinates (m)
X, Y	Dimensionless coordinates

Greek symbols

ρ	Density (kg m^{-3})
α	Thermal diffusivity (m^2 s^{-1})
β	Coefficient of thermal expansion (K^{-1})
ν	Kinematic viscosity (m^2 s^{-1})
θ	Dimensionless temperature

Subscripts

H	Hot
C	Cold
h	High
l	Low
o	Reference
S	Solutal
T	Thermal

1 Introduction

The heat and mass transport with mixtures have extensively studied in the last years within different simple/complex shape cavities. In recent review papers, a comprehensive summary of the flow and heat transfer in different shapes of cavities under different physics is presented [1, 2]. This noticeable focus is due to its important role in various engineering systems like geothermal energy, the processing of foods, electronic cooling equipment, and the applications of solar energy and building heating [3–8].

Sun et al. [9] studied the variations of large density of binary mixtures influences on double-diffusive convective flow in a square cavity. The mathematical model based on low Mach number formulation has been used in their numerical study. The results showed that, for light gases, the effects of variable density for diffusion are too important compared with their impacts on the diffusion of heavy gases. Double-diffusive natural convective transfer of heat and mass in vertical annuluses has been examined numerically by Chen et al. [10] with opposing concentration and temperature gradients. The simple LBM has been used

in their study. The Nu_{avg} and Sh_{avg} on the inner vertical wall increase by increasing Ra, AR, and radius ratio (K) for N>1. For high Ra (i.e., $Ra>10^7$), the fluid flow transient was difficult to study before, while became readily studied by using the LBM model. Also, Chen et al. [11] examined the double-diffusive free convective turbulent fluid flow in a square cavity by employing the model of LES-based lattice Boltzmann. They found a power-law correlation equation of Nu with Ra and N. Three dimension of double-diffusive heat convection in a cuboid has been examined numerically by Chen et al. [12]. The parameters $10 \leq Ra \leq 2 \times 10^5$, $2 \leq Le \leq 1000$,, and $-2 \leq N \leq 0$ are considered. An important investigation of double-diffusive convective binary mixture flow in a rectangular cavity was made by Qin et al. [13]. An AR = 2 has been considered in this study, and the horizontal walls were supplied to different gradients of the temperature and concentration. Their numerical results were in high accuracy compared with many previous studies. Jena et al. [14] analyzed numerically the transient the opposite double-diffusive natural convective flow within a square cavity. Correlation equations are developed for Nu and Sh in case of thermally dominated flow as well as solutally dominated flow. Later different correlations are developed by Corcione et al. [15] for double-diffusive free convection in square enclosures. Natural convective heat and mass transmission of Air-CO_2 mixture in a square cavity have been inspected numerically by [16–18]. The effects of partially heating vertical walls on double-diffusive natural convective non-Newtonian fluid flow have been investigated numerically by Jena et al. [19]. Reddy and Murugesan [20] investigated the cross-heat and mass transfer within a rectangular cavity with three different AR. The cavity was under the effects of mass diffusivity sidewalls, while the bottom wall was heated to high temperature and the top wall cooled to low temperature, whereas the vertical walls are adiabatic. They clarified that the Nusselt number (Nu) increases by increasing Ra and N, while the maximum Nu for the different AR (AR = 0.5, 1, and 2) was (51, 14.5, and 12,6%), respectively.

As solar thermal system applications, Chen et al. [21] inspected numerically double-diffusive natural convective nanofluid flow in a rectangular cavity with the effects of entropy generation. Kefayati and Che Sidik [22] used Buongiorno's mathematical model to investigate irreversibility in a tilted enclosure occupied with non-Newtonian nanofluid. Also, Kefayati and Tang [23] extended their previous study of double-diffusive mass and heat transfer to show the entropy generation effects [24]. Kefayati [25] studied the Dufour and Soret influences on double-diffusive free transfer of heat and mass with entropy generation in an oblique cavity filled with Bingham fluid. FDLBM has been used in his study with a wide scope of parameters involving ($10^6 \geq Ra \geq 10^3$), ($10 \geq Le \geq 2.5$), ($D_f = 0$, 1, and 5), ($S_r = 0$, 1, and 5), (Ec = 0.01, 0.001, and 0), and ($0 \geq \theta \geq 120$). His outcomes elucidated that the transfer of heat and mass increases with decreasing the Bingham number. Moreover, the transfer of heat and mass enhanced by increasing θ from (0 to 40), while the enhancement decreases when θ increases from (40 to 80). Also, he showed that the mass transfer enhanced by ascending the Soret number, and the heat transmission increases by increasing the Dufour number for different parameters. In addition, the previews works [26–31] include several numerical investigations of double-diffusive natural/mixed convective flow in the horizontal annulus.

The influences of MHD on double-diffusive heat and mass transfer with/without entropy generation have been studied by many researchers [32–37]. It is to worth mention here that besides the previously mentioned literature, rarefied flow and heat transfer in cavities are examined by different researchers [38–41].

The above literature survey indicates that much less curiosity has been paid to the problem of double diffusion in staggered cavities. The objective of the present investigation is to analyze computationally the double-diffusion natural convective flow in a staggered cavity in which there is an Air-CO_2 mixture filled the cavity. The vertical staggered cavity walls are

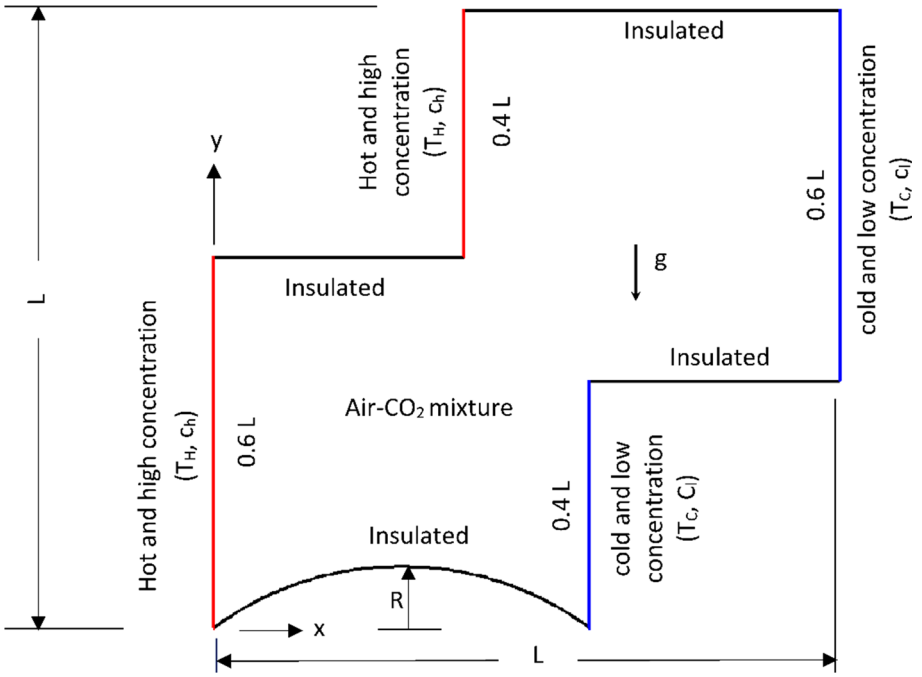

Fig. 1 Schematic for the geometry

kept with variant concentrations and temperatures, while the horizontal walls are insulated. The study has been performed with taken the impacts of numerous factors such as Rayleigh number (Ra), buoyancy ratio (N), aspect ratio (AR), and Lewis number (Le) for both aiding and opposing flows. Outcomes represented by streamlines, isotherms, iso-concentrations contours, average Nusselt number (Nu_{avg}), and average Sherwood number (Sh_{avg}) plots have been discussed in the next sections.

2 Problem description

The configuration of the present study is represented by a staggering cavity as shown in Fig. 1. The cavity is containing Air-CO_2 mixture, and its side walls are maintained with different concentrations and temperatures, in which the cavity left side walls have a hot temperature (T_H) and higher concentration (c_h), while the cavity right side walls have a cold temperature (T_C) and lower concentration (c_l). The cavity remaining walls involving the lower arc are maintained as impermeable and insulated. The Air-CO_2 mixture flow within the cavity is presumed to be laminar, incompressible, steady, and governed by Boussinesq approximation. The cavity has an equal length (L) and height (L), while the arc radius is (R).

3 Governing equations

Based on the physical description in the last section, the mass, momentum, energy, and species conservation equations are represented as follows [42]:

Table 1 Air-CO_2 mixture properties [4]

ρ_o (kg.m^{-3})	$C_{p,o}$ (J.kg^{-1}.K^{-1})	k_o (W.m^{-1}.K^{-1})	μ_o (kg.m^{-1}.s^{-1})	D (m^2.s^{-1})
1.16	1006.9	2.63×10^{-2}	1.85×10^{-5}	2.25×10^{-5}

$$\frac{\partial u}{\partial x} + \frac{\partial v}{\partial y} = 0 \tag{1}$$

$$u\frac{\partial u}{\partial x} + v\frac{\partial u}{\partial y} = -\frac{1}{\rho}\frac{\partial p}{\partial x} + \nu\left(\frac{\partial^2 u}{\partial x^2} + \frac{\partial^2 u}{\partial y^2}\right) \tag{2}$$

$$u\frac{\partial v}{\partial x} + v\frac{\partial v}{\partial y} = -\frac{1}{\rho}\frac{\partial p}{\partial y} + \nu\left(\frac{\partial^2 v}{\partial x^2} + \frac{\partial^2 v}{\partial y^2}\right) + [\beta_T(T - T_C) + \beta_S(c - c_l)]g \tag{3}$$

$$u\frac{\partial T}{\partial x} + v\frac{\partial T}{\partial y} = \alpha\left(\frac{\partial^2 T}{\partial x^2} + \frac{\partial^2 T}{\partial y^2}\right) \tag{4}$$

$$u\frac{\partial c}{\partial x} + v\frac{\partial c}{\partial y} = D\left(\frac{\partial^2 c}{\partial x^2} + \frac{\partial^2 c}{\partial y^2}\right) \tag{5}$$

The thermophysical properties for Air-CO_2 mixture are illustrated in Table 1.

The density in Eqs. (1−5) is varying reference to the Boussinesq approximation as follows:

$$\rho = \rho_o[1 - \beta_T(T - T_C) + \beta_S(c - c_l)] \tag{6}$$

where ρ_o is the density of fluid at the reference temperature $T_o = (T_H + T_C)/2$ and concentration $c_o = (c_h + c_l)/2$, while $\beta_T = -\left(1/\rho_o\right)\left(\partial\rho/\partial T\right)_S$ and $\beta_S = -\left(1/\rho_o\right)\left(\partial\rho/\partial c\right)_T$ are the thermal and solute expansion coefficients, respectively.

The boundary conditions for each wall can be given as:

for aiding flow:

$$T = T_H,\ c = c_l \quad \text{at the left vertical walls.}$$

$$T = T_C,\ c = c_h \quad \text{at the right vertical walls.}$$

for opposing flow:

$$T = T_H,\ c = c_h \quad \text{at the left vertical walls.}$$

$$T = T_C,\ c = c_l \quad \text{at the right vertical walls.}$$

The arc and all horizontal walls are:

$$\frac{\partial T}{\partial y} = 0,\ \frac{\partial c}{\partial y} = 0$$

The foregoing equations can be written in non-dimensional form utilizing the next non-dimensional factors:

$$X = \frac{x}{L}, \quad Y = \frac{y}{L}, \quad U = \frac{uL}{\alpha}, \quad V = \frac{vL}{\alpha}, \quad P = \frac{pL^2}{\rho\alpha^2}, \quad \theta = \frac{T - T_C}{T_H - T_C},$$
$$C = \frac{c - c_l}{c_h - c_l}, \quad \mathrm{Pr} = \frac{\nu}{\alpha}, \quad \mathrm{Le} = \frac{\alpha}{D},$$
$$\mathrm{Ra} = \frac{g\beta_T(T_H - T_C)L^3}{\nu\alpha}, \quad \mathrm{N} = \frac{\beta_S(c_h - c_l)}{\beta_T\,(T_H - T_C)}, \quad \mathrm{AR} = \frac{R}{L}.$$

Hence, in the light of assumption all Eqs. (1−5) can be reformulated into dimensionless as follows:

$$\frac{\partial U}{\partial X} + \frac{\partial V}{\partial Y} = 0 \tag{7}$$

$$U\frac{\partial U}{\partial X} + V\frac{\partial U}{\partial Y} = -\frac{\partial P}{\partial X} + Pr\left(\frac{\partial^2 U}{\partial X^2} + \frac{\partial^2 U}{\partial Y^2}\right) \tag{8}$$

$$U\frac{\partial V}{\partial X} + V\frac{\partial V}{\partial Y} = -\frac{\partial P}{\partial Y} + Pr\left(\frac{\partial^2 V}{\partial X^2} + \frac{\partial^2 V}{\partial Y^2}\right) + RaPr\left(\theta + Le^{-1}NC\right) \tag{9}$$

$$U\frac{\partial \theta}{\partial X} + V\frac{\partial \theta}{\partial Y} = \left(\frac{\partial^2 \theta}{\partial X^2} + \frac{\partial^2 \theta}{\partial Y^2}\right) \tag{10}$$

$$U\frac{\partial C}{\partial X} + V\frac{\partial C}{\partial Y} = Le^{-1}\left(\frac{\partial^2 C}{\partial X^2} + \frac{\partial^2 C}{\partial Y^2}\right) \tag{11}$$

The boundary conditions can be expressed in dimensionless form as:
for aiding flow:

$$\theta = 1,\ C = 0 \quad \text{at the left vertical walls.}$$

$$\theta = 0,\ C = 1 \quad \text{at the right vertical walls.}$$

for opposing flow:

$$\theta = 1,\ C = 1 \quad \text{at the left vertical walls.}$$

$$\theta = 0,\ C = 0 \quad \text{at the right vertical walls.}$$

The arc and all horizontal walls are:

$$\frac{\partial \theta}{\partial Y} = 0, \quad \frac{\partial C}{\partial Y} = 0$$

The mean Nusselt number ($\mathrm{Nu_{avg}}$) expressing the rate of heat transfer on the cavity side walls can be defined as:

$$\mathrm{Nu_{avg}} = -\int_0^1 \frac{\partial \theta}{\partial X} dY \tag{12}$$

The mean Sherwood number ($\mathrm{Sh_{avg}}$) expressing the rate of mass transfer within the cavity side walls can be defined as:

$$\mathrm{Sh_{avg}} = -\int_0^1 \frac{\partial C}{\partial X} dY \tag{13}$$

4 Solution procedure

The governing relations with the boundary conditions mentioned in the preceding section are numerically solved by the finite volume procedure. The SIMPLEC algorithm is utilized to link the continuity and momentum relations. PRESTO (pressure-staggering-option) scheme is employed to discretize the pressure. Moreover, the upwind second order is chosen as an interpolation scheme for energy, momentum, and species relations. The solution of the discretized pressure and momentum relations is obtained using the method of Patankar [43]. Iteration method is started by solving the momentum relations pursued by energy and species relations. The solution proceeds till convergence is attained when all dependent parameters reach an accuracy of 10^{-6}.

5 Grid independence and verification

The grids type employed in the present study is uniform quadrilateral grids as exhibited in Fig. 2. In order to examine the grid quality, six grid numbers have been employed. Nu_{avg} on the left vertical cavity walls is presented at these six grid numbers as depicted in Table 2. The table revealed that Nu_{avg} is altered as the grid numbers enlarge and Nu_{avg} values are no longer varied with the higher grid numbers 19961 and 22031, which indicates constancy in

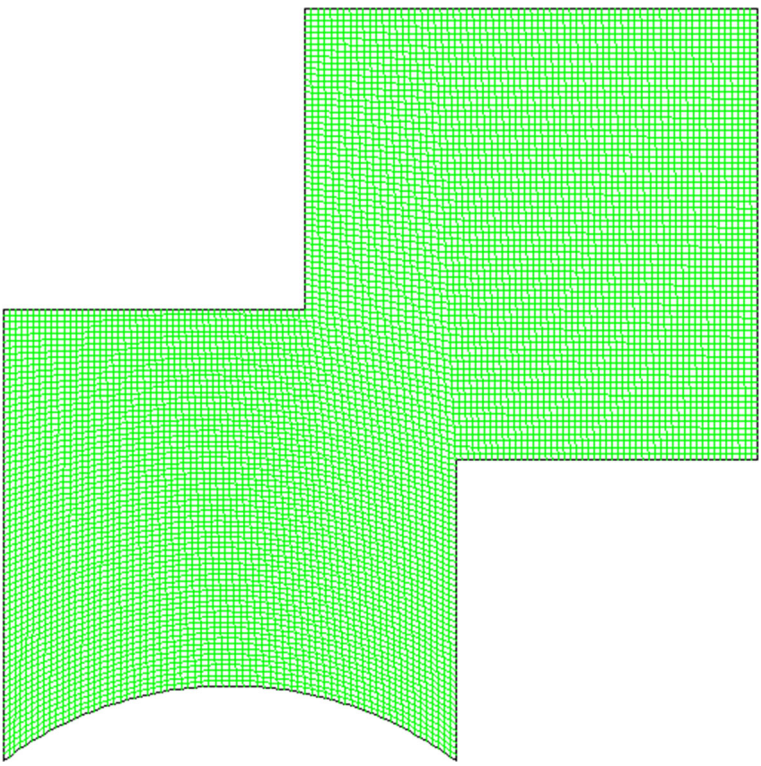

Fig. 2 Mesh utilized in the computations

Table 2 Grid dependency N = 2, Ra = 10^6, Le = 1, AR = 0.1

No.	Grid number	Nu_{avg} (Sh_{avg})
1	7001	11.221
2	9641	11.133
3	12,681	11.084
4	16,121	11.045
5	19,961	11.026
6	22,031	11.026

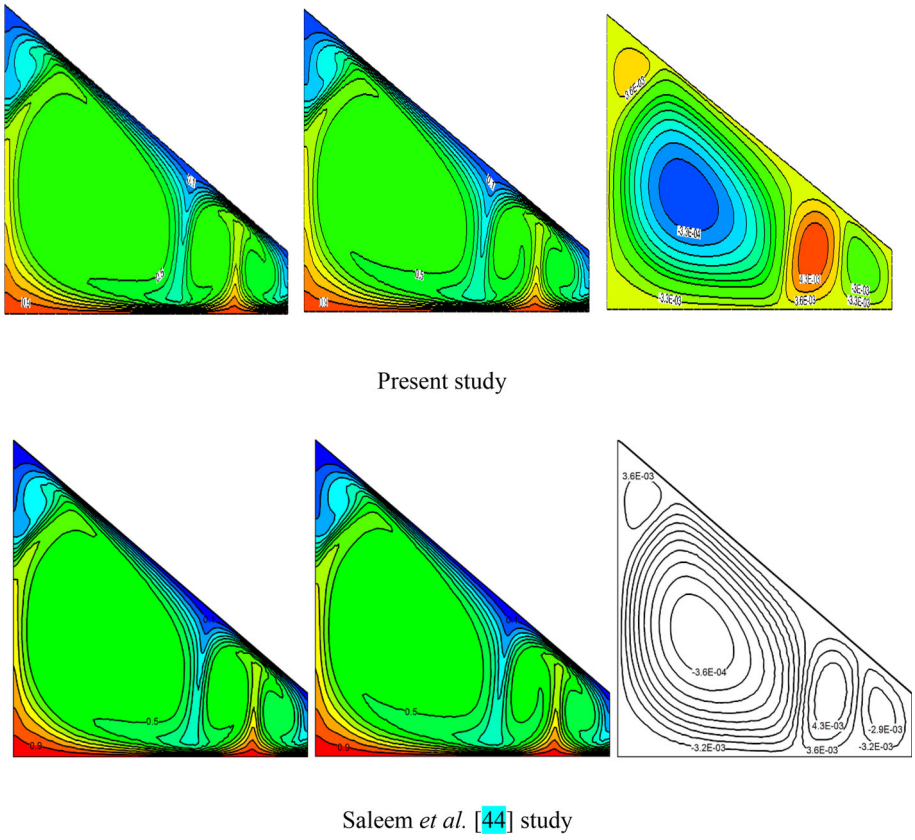

Fig. 3 Isotherms (left), iso-concentration lines (middle), and streamlines (right) comparison between the current study and Saleem et al. [44] with Ra = 10^6, N = 2, $Re_\infty = 10^4$, and Le = 0.89

outcomes reached with these grid values. The grid number 19961 has been selected in the calculations because it takes less time to run and gives similar results as the highest number.

For verification of results, the present model is compared with two different cases from the literature. In Fig. 3, the current model is configured to the case of Saleem et al. [44], which they deemed a solar distiller its side walls differentially heated and kept with variant concentrations with Ra = 10^6, N = 2, and $Re_\infty = 10^4$. The figure exhibited that there is a very good concordance between the present model and Saleem et al. [44] outcomes. In Fig. 4a and b, the present model compared with a square cavity its sidewalls maintained with variant

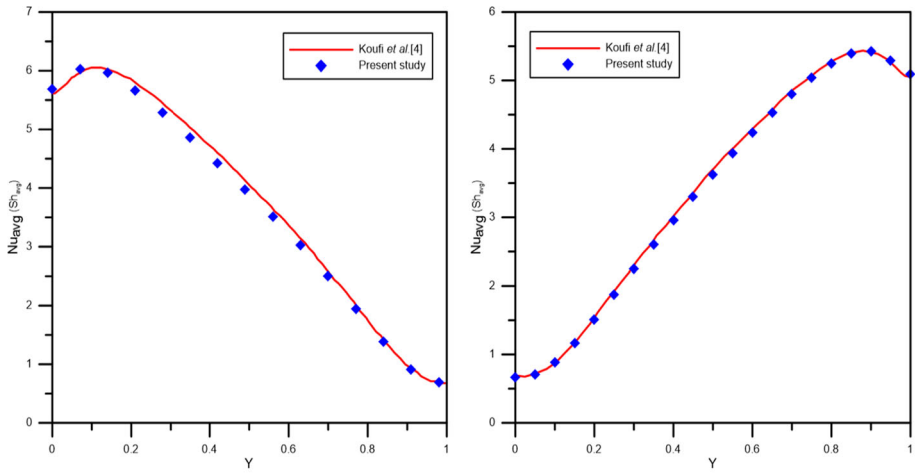

Fig. 4 Comparison of Nu_{avg} (Sh_{avg}) for the current study and Koufi et al. [4] outcomes with $Ra = 10^4$ and $Le = 1$

temperature and concentration with $Le = 1$, $Ra = 10^4$ with $N = 5$ (aided flow) and $N = -5$ (opposing flow) as taken by Koufi et al. [4]. Values of Nu_{avg} (Sh_{avg}) have been predicted on the left side cavity walls. In the figure Le is deemed as unity, then $Nu_{avg} = Sh_{avg}$. It is obvious from the figure that the outcomes from the present study accurately coincide with Koufi et al. [4] predictions, that is reflecting the validity of the present study in solving heat and mass transfer in numerous enclosures.

6 Results and discussion

In the current paper, calculations have been achieved with the following scopes of parameters: $Ra = 10^4$,10^5, and 10^6; $N = -1, -2, -3, -5, 1, 2, 3$, and 5; $Le = 1$, 3, and 5; $AR = 0.1$, 0.15, and 0.2, while Pr is assumed to be fixed at 0.7. The impact of Ra, N, Le, and AR on the streamlines, isotherms, iso-concentration lines, Nu_{avg}, and Sh_{avg}, will be discussed in the next figures.

Figure 5 exhibits the isotherms, iso-concentration lines, and streamlines for the aiding flow case where $N = 1$, AR is fixed to 0.1, $Le = 1$, and different Ra. In general, the plots reveal that the flow is symmetric. Moreover, the graph depicts that the higher isotherms values are at and near the hot cavity walls, and the lower isotherms values are located at or near the cold cavity walls. As far as the movement of the fluid inside the cavity is concerned, at low Ra, the cavity has two vortices, one in the upper cavity part and the other one is in the lower cavity part. When the Ra increases, the upper vortex increases in size and distortion of the streamlines occurs; mainly this is because the recirculation happens inside the cavity, and this recirculation is in the clockwise direction. For $Ra = 10^6$, the two vortices merge to form a central big vortex at the middle of the cavity. The recirculation happens due to two main factors, one is the air density difference that is induced by the temperature and the second one is the CO_2 gradients nearby of the cavity walls. Finally, it is worth mentioning here that the iso-concentration lines are identical to the isotherms except for the fact that the maximum

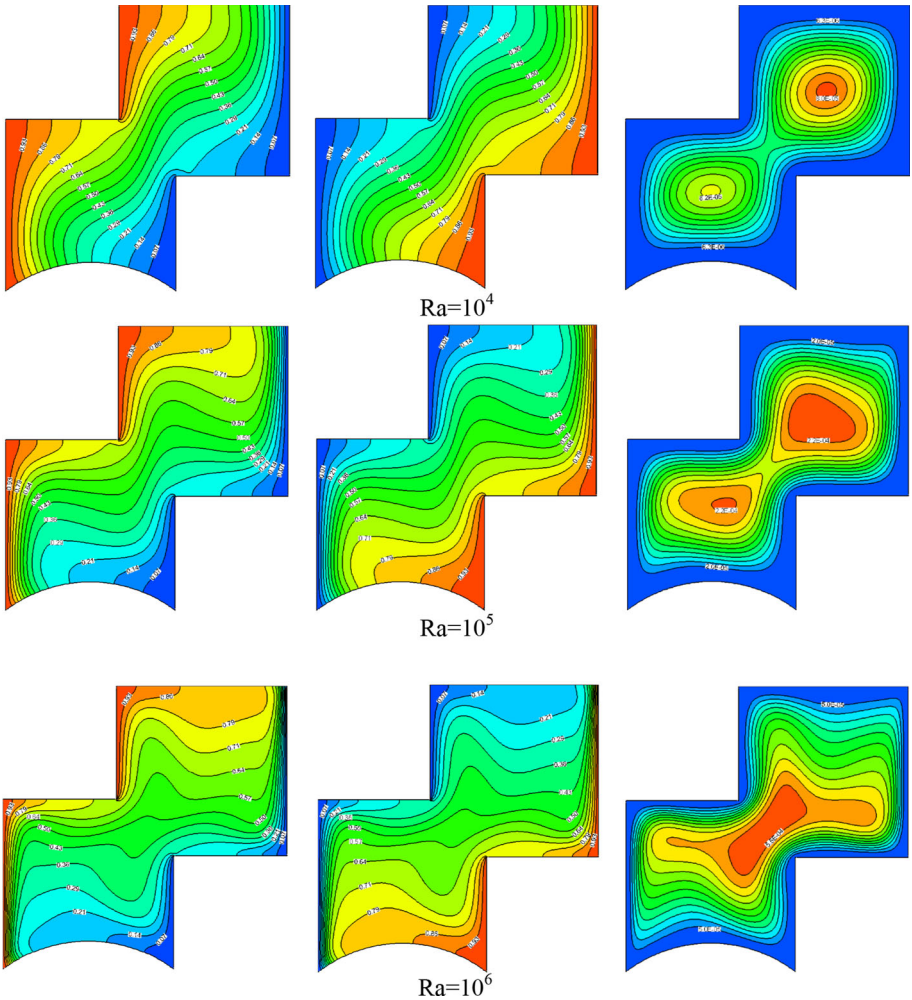

Fig. 5 Isotherms (left), iso-concentration lines (middle), and streamlines (right) for N = 1, AR = 0.1, and Le = 1 for distinct Ra values

values are observed near the vicinity of the cavity right walls, while the lower values are at the vicinity of the hot walls of the cavity.

In Fig. 6, the isotherms, iso-concentration, and the streamlines are plotted for the opposing flow where N = − 1, AR = 0.1, Le = 1, and different Ra. In these cases, the highest temperatures and concentration of CO_2 are located at the left cavity walls, while the lower values are at the right cavity walls. It is seen from the plots that both of the isotherms and iso-concentration lines are identical. Moreover, it is obvious that the solute and thermal buoyancy forces are totally cancelled. Furthermore, the convective heat transfer vanishes and the transfer of mass and heat occurs mainly due to diffusion with a monotonic temperature. Moreover, through the vertical walls, the concentration distributions are completely stratified. The graph also shows that there is no boundary layer existing. Additionally, it is obvious that the iso-concentration lines and the isotherms are almost vertical and parallel. As far as the

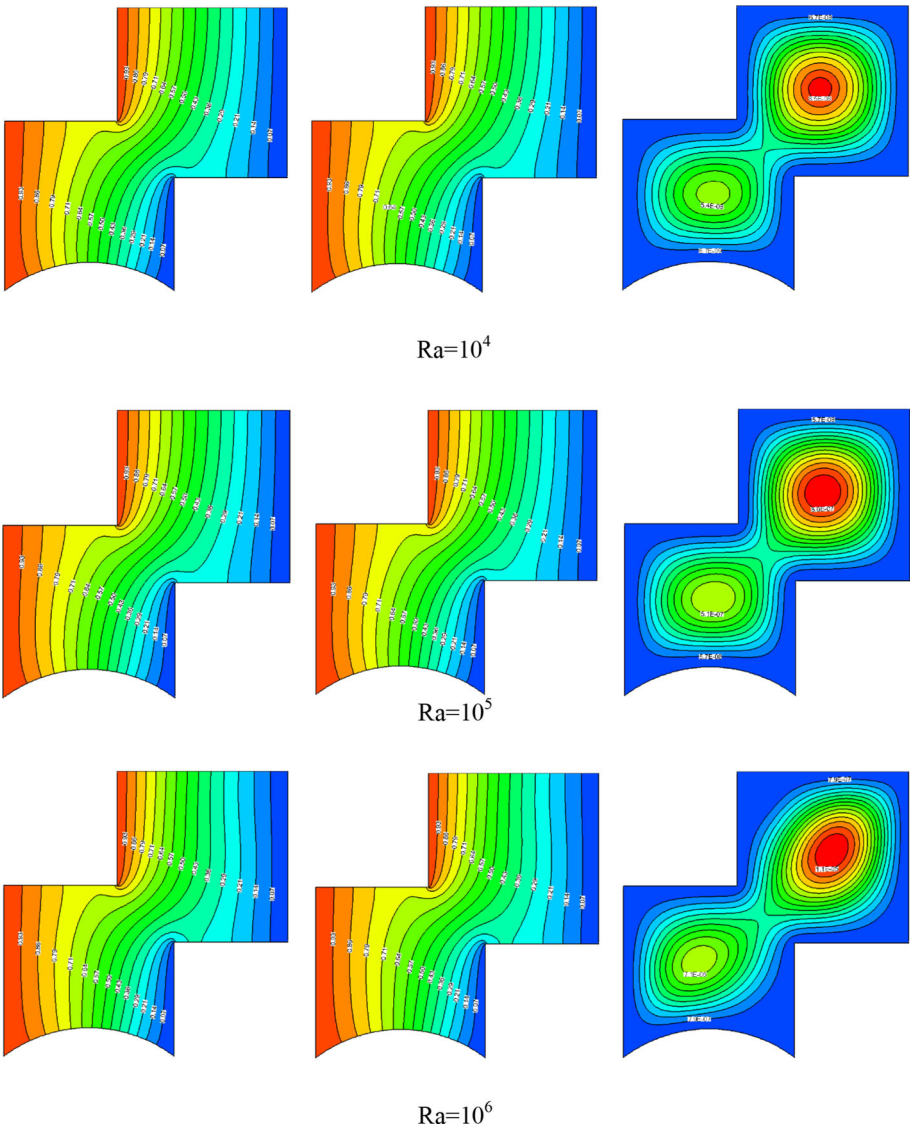

Fig. 6 Isotherms (left), iso-concentration lines (middle), and streamlines (right) for N = − 1, AR = 0.1, and Le = 1 for distinct Ra values

streamlines are concerned, the flow breaks into two structures at the upper and lower parts of the cavity. Finally, when Ra increases, more distortion happens to these lines.

Figure 7 depicts the variations of the isotherms, iso-concentration lines, and the streamlines for the aiding flow case where $Ra = 10^5$, Le = 1, and different N ranging from 1 to 5. The same observations of Fig. 5 are noticed for the higher and lower values. It is worth mentioning here that increasing N will not significantly affect the isotherms and the iso-concentration lines. Moreover, the isotherms and the iso-concentration lines share the same tendency. These are vertical at the boundary layer and horizontal at the middle of the cavity. Concerning the

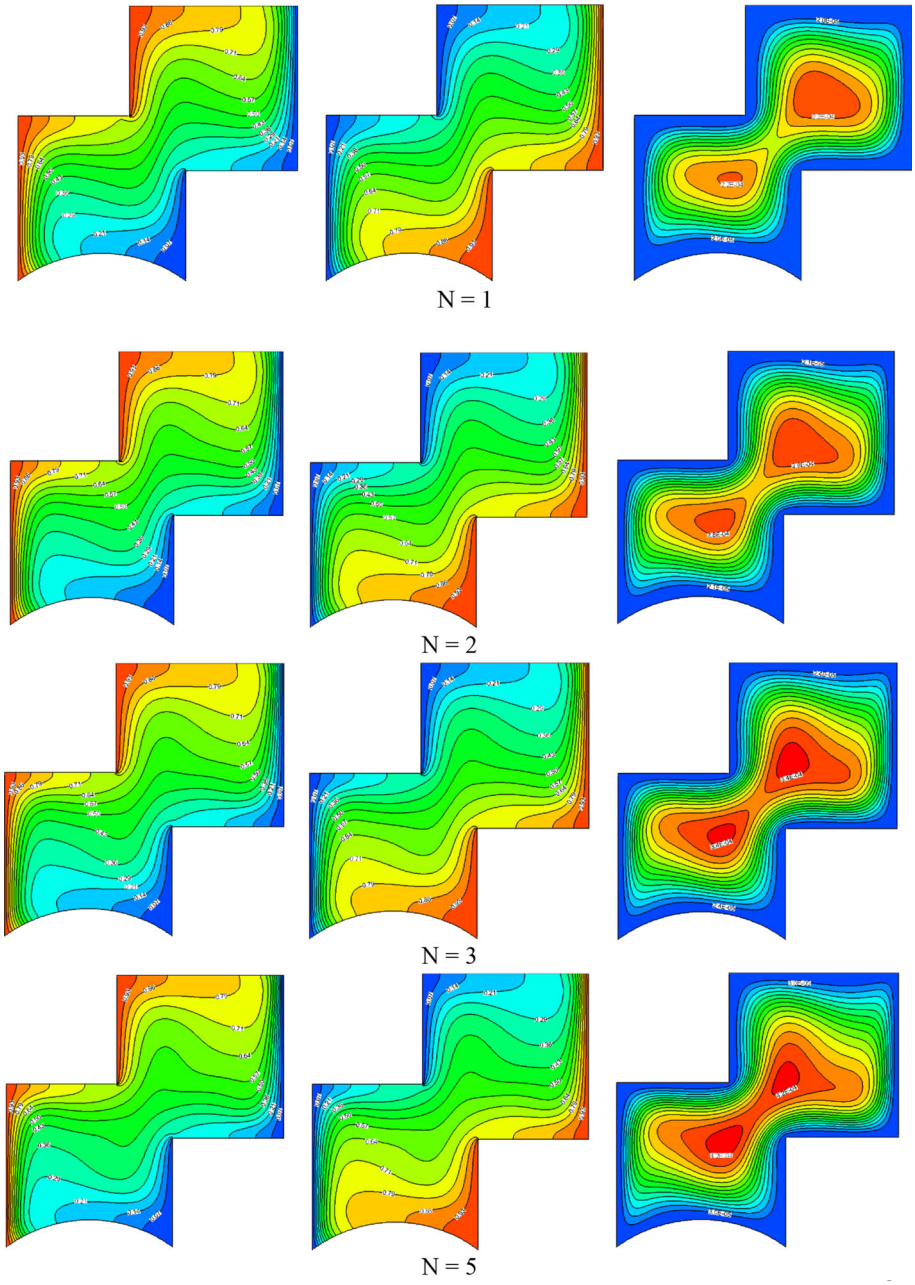

Fig. 7 Isotherms (left), iso-concentration lines (middle), and streamlines (right) for Ra $= 10^5$, AR $= 0.1$, and Le $= 1$ for numerous N values (aiding flow)

streamlines, as N ascents, the flow movement augments. This is an indication that the flow is accelerating. The movement of the mixture is aided by the solutal and buoyancy forces.

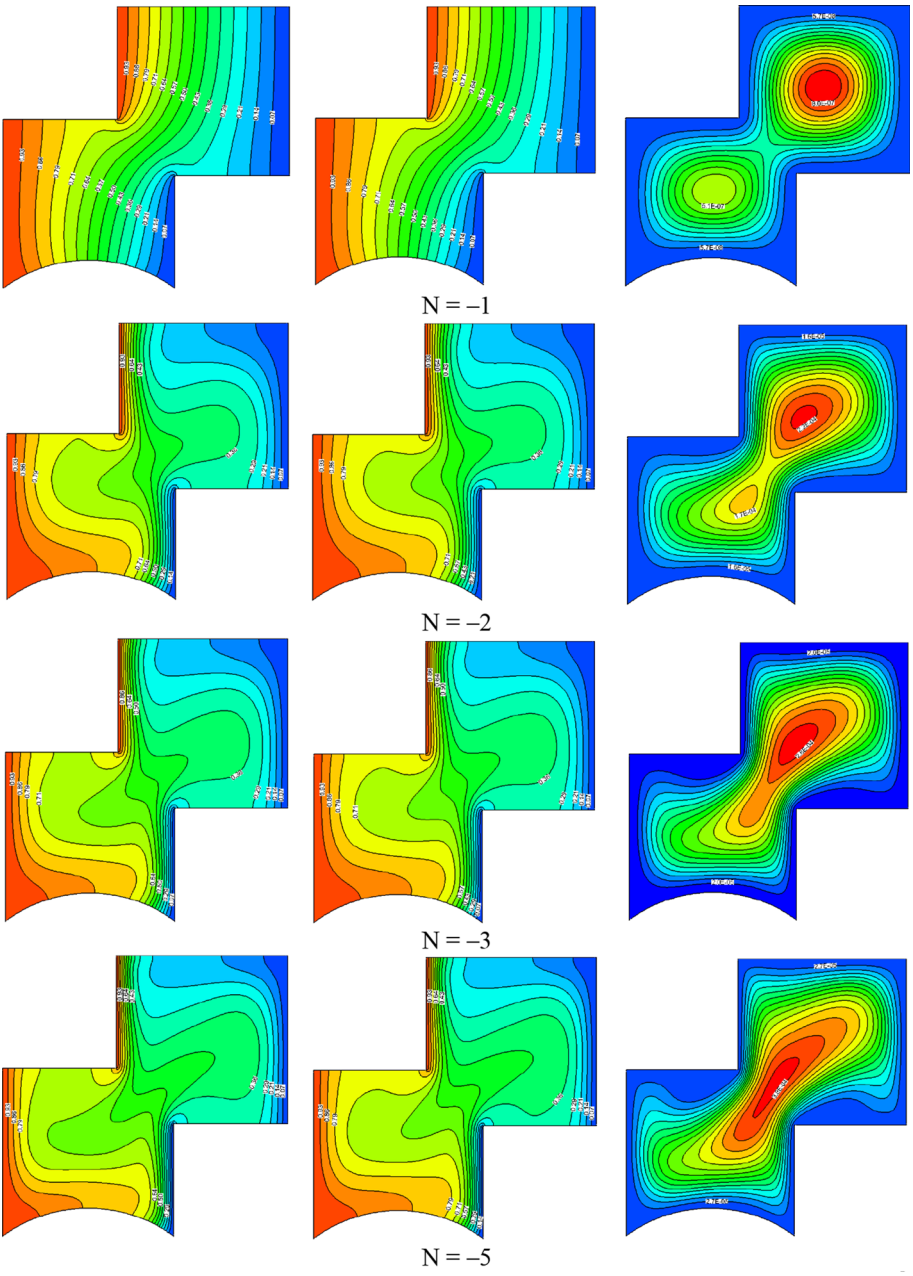

Fig. 8 Isotherms (left), iso-concentration lines (middle), and streamlines (right) for Ra $= 10^5$, AR $= 0.1$, and Le $= 1$ for numerous N values (opposing flow)

In Fig. 8, the variations of the isotherms, iso-concentration lines, and the streamlines are illustrated for the opposing case where Ra $= 10^5$, Le $= 1$, and different N varying from -1 to -5. For cases where N is less than -1, the thermal buoyancy force is less than the solute

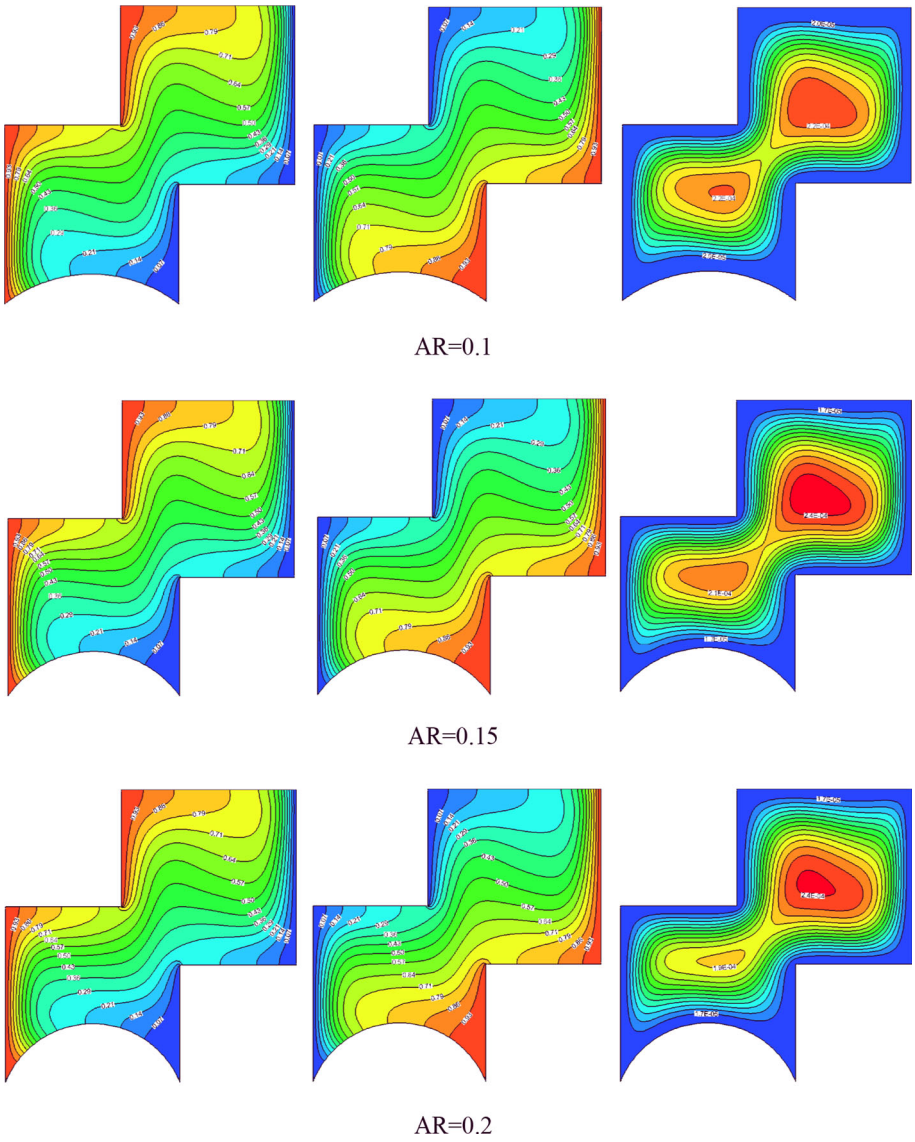

Fig. 9 Isotherms (left), iso-concentration lines (middle), and streamlines (right) for N = 1, Ra = 10^5, and Le = 1 for numerous AR values

buoyancy force. Thus, the fluid motion is mainly controlled by the solutal free convection with a counterclockwise direction. Moreover, as N decreases, the two vortices in the upper and lower cavity parts merge to form one cell in the middle of the cavity for the case where N = − 5.

It can be concluded from the discussion of the previous figures that the best scenario of having a significant enhancement in heat transfer is a combination of high Ra and high positive N.

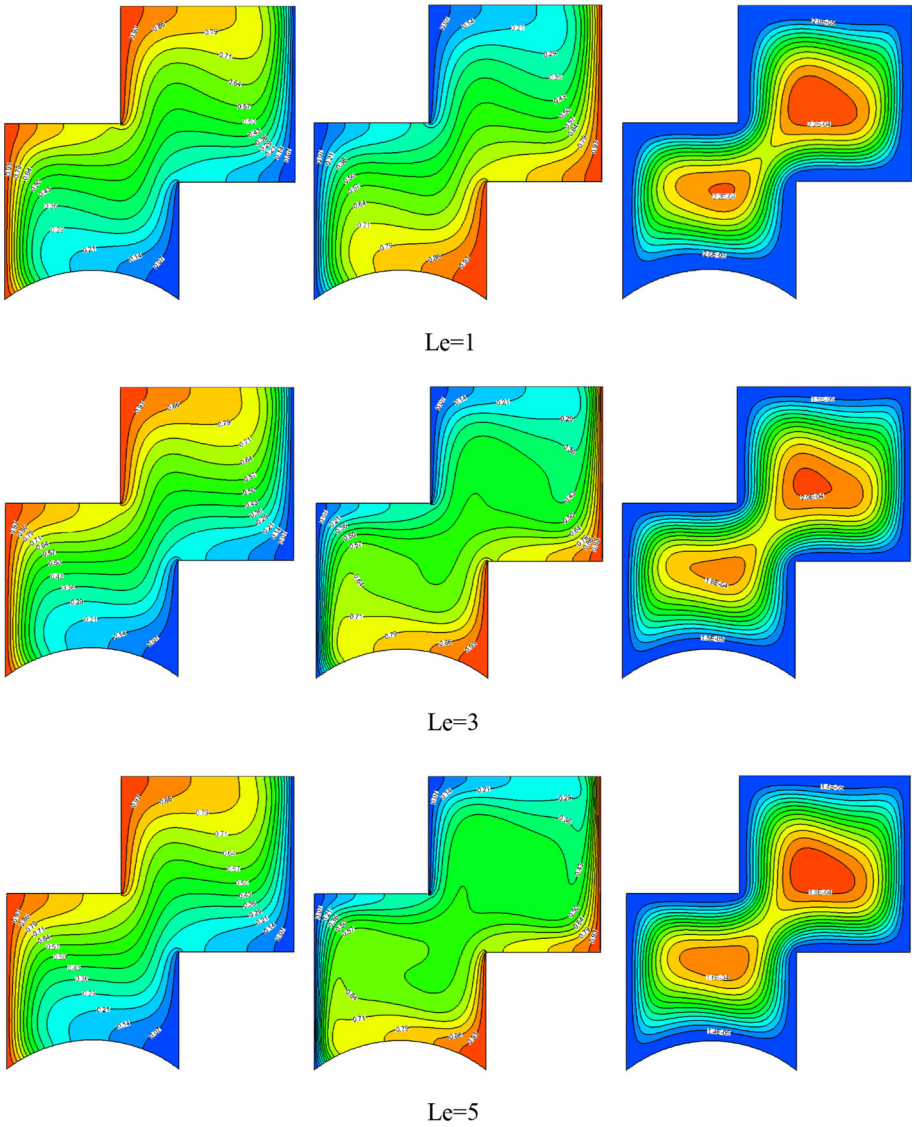

Fig. 10 Isotherms (left), iso-concentration lines (middle), and streamlines (right) for N = 1, AR = 0.1, and Ra = 10^5 for distinct Le values

Figure 9 depicts the variations in isotherms, iso-concentrations, and streamlines for the cases where Ra = 10^5, Le = 1, N = 1, and different AR. The same discussion of Fig. 5 is applied to this figure. Moreover, it can be seen that the fluid movement within the cavity is more restricted as AR increases. Hence, the increase in AR will decrease the heat transfer, and consequently, less Nu_{avg} is achieved.

Figures 10 and 11 represent variations of the isotherms, iso-concentration lines, and streamlines for aiding and opposing flows, respectively. The cases are taken for Ra = 10^5, AR = 0.1, and different Le. The same discussion in Figs. 5 and 6 is applied here for Figs. 10

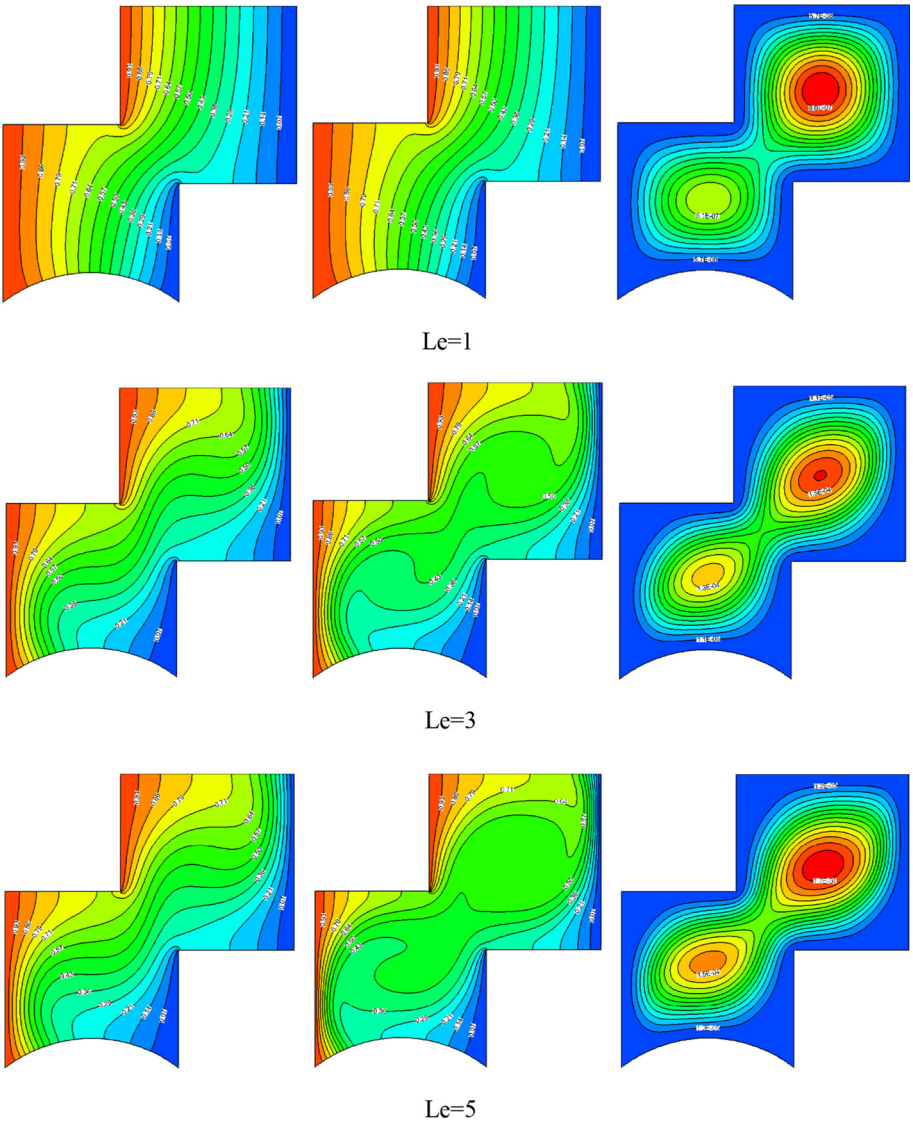

Fig. 11 Isotherms (left), iso-concentration lines (middle), and streamlines (right) for N = − 1, AR = 0.1, and Ra = 10^5 for distinct Le values

and 11, respectively. Moreover, for the case of the aiding flow and different Le, it is seen that as Le ascends, the intensity of the movement of the fluid diminishes and hence less Nu_{avg} is achieved. Finally, for the opposing flow, as Le increases, the movement of the flow increases within the cavity, and consequently, a better transfer of heat is achieved.

Figure 12 illustrates variations of Nu_{avg} (Sh_{avg}) with N at different Ra, Le = 1, and AR = 0.1 for the aiding flow. The graph shows that as Ra increases, better heat transfer is achieved. This is because as Ra increases, the convective transfer of heat becomes the prevailing mode of heat transmission inside the cavity. Furthermore, the graph exhibits that as N ascends

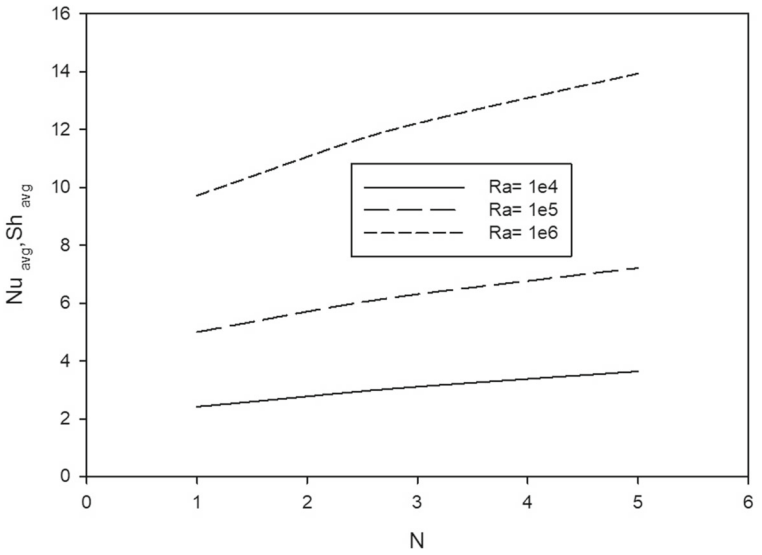

Fig. 12 Variations of the Nu_{avg}, Sh_{avg} with N (aiding flows) for different Ra

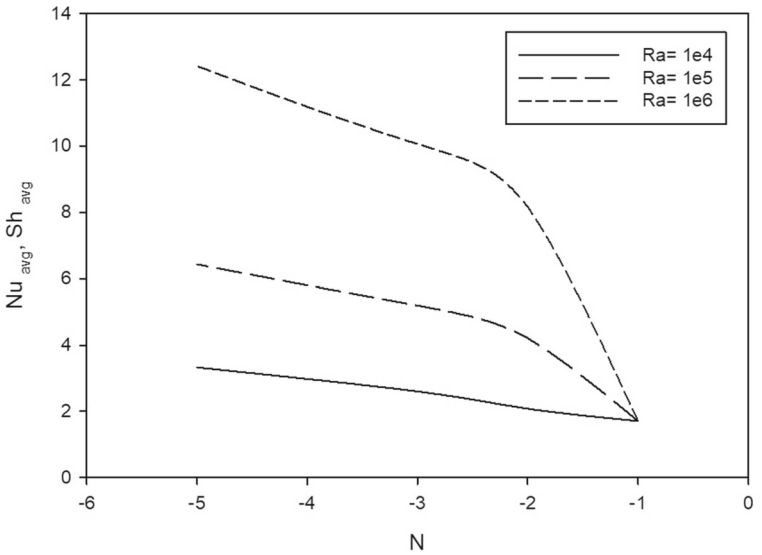

Fig. 13 Variations of the Nu_{avg}, Sh_{avg} with N (opposing flows) for different Ra

for the aiding flow, Nu_{avg} (Sh_{avg}) increases. In Fig. 13, variations of Nu_{avg} (Sh_{avg}) with N at different Ra, Le = 1, and AR = 0.1 for the opposing flow are shown. Similarly, as Ra increases, Nu_{avg} (Sh_{avg}) increases. Moreover, as N decreases for the opposing flow, Nu_{avg} (Sh_{avg}) increases. Moreover, the figure revealed that Ra has less impact on Nu_{avg} (Sh_{avg}) when N = -1.

Figure 14 confirms the conclusion drawn in Fig. 9. It is clear to show that when AR increases, both of the Nu_{avg} and Sh_{avg} decrease for the case where $Ra = 10^5$ and N = 1. The

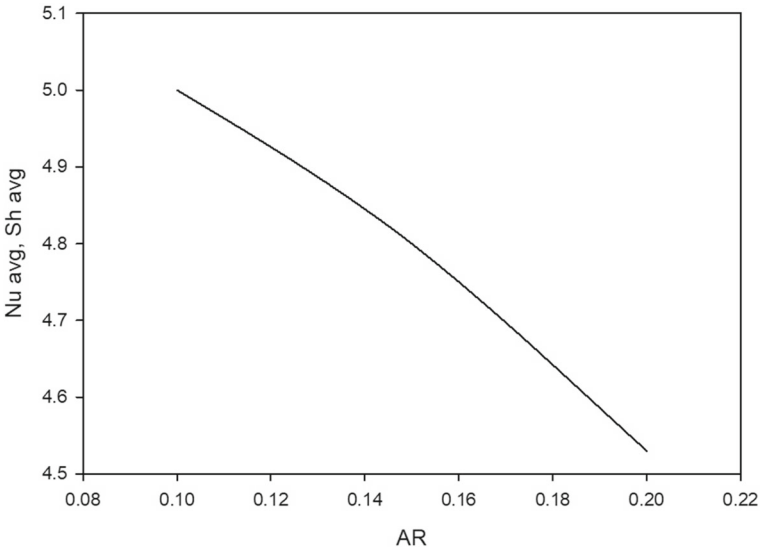

Fig. 14 Variations of the Nu_{avg}, Sh_{avg} with AR for aiding flow

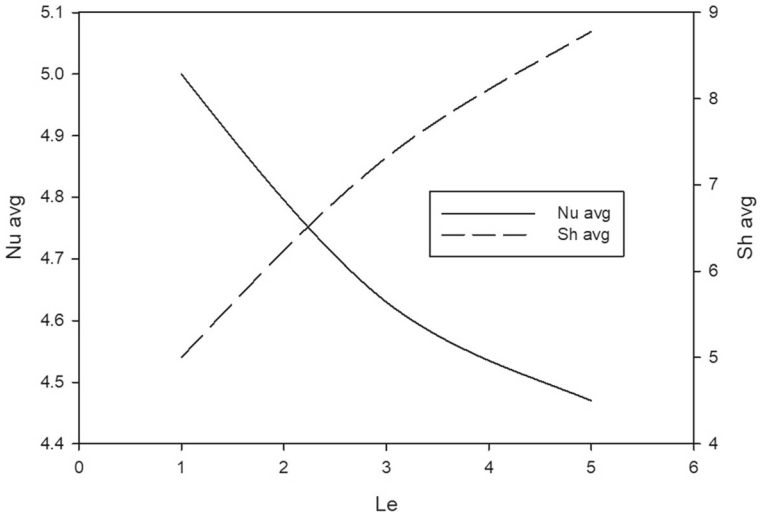

Fig. 15 Variations of the Nu_{avg}, Sh_{avg} with Le for aiding flow

depression in Nu_{avg} (Sh_{avg}) between the lower and higher AR values is 10.4%. Similarly, Figs. 15 and 16 emphasize the results obtained in Figs. 10 and 11, respectively. For the aiding flow, as Le increases, Nu_{avg} decreases and Sh_{avg} increases. Finally, for the opposing flow, as Le increases, both Nu_{avg} and Sh_{avg} increase.

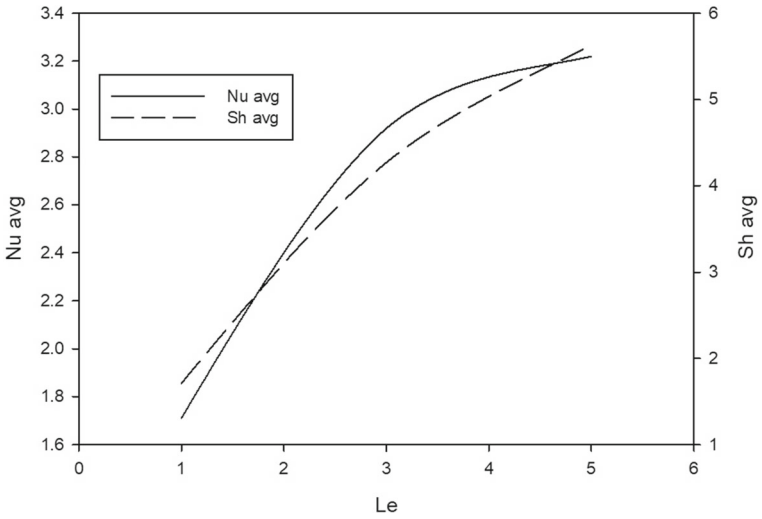

Fig. 16 Variations of the Nu_{avg}, Sh_{avg} with Le for opposing flow

7 Conclusions

A double-diffusion two-dimensional steady-state and laminar natural convection in staggered cavities with concaved lower wall is investigated. The finite volume scheme is employed to solve the governing equations along with the boundary conditions. Impacts of aspect ratio (AR), Lewis number (Le), buoyancy ratio (N), and Rayleigh number (Ra) on the flow characteristics are investigated and presented as isotherms, streamlines, and iso-concentration. Moreover, variations of the average Nusselt number (Nu_{avg}) and average Sherwood number (Sh_{avg}) with these parameters are analyzed and discussed thoroughly. The following conclusions are remarked:

- Ascending of Ra lessens the number of vortices inside the cavity for the aiding flow. In contrast, with the opposing flow, the number of vortices still fixed as Ra rises.
- For aiding flow, N has less impact on the iso-concentration lines and isotherms.
- For opposing flow, Ra has no impact on the isotherms and iso-concentration lines.
- Enlarge of AR lessens the fluid motion inside the cavity.
- Both Nu_{avg} and Sh_{avg} ascend with rising N and Ra for the aiding flows. These also are found to increase with increasing N for the opposing flows.
- AR has an inverse relationship with Nu_{avg} and Sh_{avg}.
- For the aiding flow, as Le increases, Nu_{avg} decreases and Sh_{avg} increases, while, for the opposing flow, as Le increases, both of Nu_{avg} and Sh_{avg} increase.

Funding No funding was received to assist with the preparation of this manuscript.

References

1. A.A. Hussien, W. Al-kouz, M.E. Hassan et al., A review of flow and heat transfer in cavities and their applications. Eur. Phys. J. Plus **136**, 353 (2021). https://doi.org/10.1140/epjp/s13360-021-01320-3
2. A. Abdulkadhim, K. Al-Farhany, A.M. Abed, H.S. Majdi, Al-Qadisiyah J. Eng. Sci. **13**, 80 (2020)

3. A. Ababaei, M. Abbaszadeh, A. Arefmanesh, A.J. Chamkha, Numer. Heat Transf. Part A Appl. **73**, 702 (2018)
4. L. Koufi, Y. Cherif, Z. Younsi, H. Naji, Heat Transf. Eng. **40**, 1268 (2019)
5. S. Chen, Appl. Math. Comput. **217**, 217–226 (2011).
6. Z. Alloui, H. Beji, P. Vasseur, Comput. Math. Appl. **62**, 725 (2011)
7. R. Alvarado-Juárez, G. Álvarez, J. Xamán, I. Hernández-López, Desalination **325**, 84 (2013)
8. T. Bao, Z. (Leo) Liu, Appl. Energy **237**, 566 (2019)
9. H. Sun, G. Lauriat, D.L. Sun, W.Q. Tao, Int. J. Heat Mass Transf. **53**, 615 (2010)
10. S. Chen, J. Tölke, M. Krafczyk, Int. J. Heat Fluid Flow **31**, 217 (2010)
11. S. Chen, H. Liu, C. Zheng, Int. J. Heat Mass Transf. **55**, 4862 (2012)
12. Z.W. Chen, J.M. Zhan, Y.S. Li, Y.Y. Luo, S. Cai, Int. J. Heat Mass Transf. **60**, 422 (2013)
13. Q. Qin, Z.A. Xia, Z.F. Tian, Int. J. Heat Mass Transf. **71**, 405 (2014)
14. S.K. Jena, L.K. Malla, S.K. Mahapatra, A.J. Chamkha, Int. J. Heat Mass Transf. **81**, 681 (2015)
15. M. Corcione, S. Grignaffini, A. Quintino, Int. J. Heat Mass Transf. **81**, 811 (2015)
16. J. Serrano-Arellano, J. Xamán, G. Álvarez, M. Gijón-Rivera, Int. J. Heat Mass Transf. **64**, 725 (2013)
17. J. Serrano-Arellano, M. Gijón-Rivera, Int. J. Heat Mass Transf. **70**, 103 (2014)
18. J. Serrano-Arellano, M. Gijón-Rivera, J.M. Riesco-Ávila, F. Elizalde-Blancas, Int. J. Heat Mass Transf. **71**, 664 (2014)
19. S.K. Jena, S.K. Mahapatra, A. Sarkar, A.J. Chamkha, J. Taiwan Inst. Chem. Eng. **51**, 9 (2015)
20. N. Reddy and K. Murugesan, Front. Heat Mass Transf. **8**, 7 (2017)
21. S. Chen, B. Yang, X. Xiao, C. Zheng, Int. J. Heat Mass Transf. **87**, 477 (2015)
22. G.H.R. Kefayati, N.A. Che Sidik, Powder Technol. **305**, 679 (2017)
23. G.R. Kefayati, H. Tang. Double-diffusive natural convection and entropy generation of Carreau fluid in a heated enclosure with an inner circular cold cylinder (Part I: Heatand mass transfer). Int. J. Heat Mass Transf. **120**, 731–750 (2018). https://doi.org/10.1016/j.ijheatmasstransfer.2017.12.080G.H.R
24. G.R. Kefayati, H. Tang. Double-diffusive laminar natural convection and entropy generation of Carreau fluid in a heated enclosure with an inner circular cold cylinder (Part II: Entropy generation). Int. J. Heat Mass Transf. **120**, 683–713 (2018). https://doi.org/10.1016/j.ijheatmasstransfer.2017.12.081
25. G.H.R. Kefayati, Int. J. Heat Mass Transf. **116**, 762 (2018)
26. A.M. Al-Amiri, K.M. Khanafer, Int. J. Therm. Sci. **45**, 567 (2006)
27. W. Al-Kouz, A. Alshare, A. Alkhalidi, and S. Kiwan, Springerplus **5**, (2016)
28. M. Ghalambaz, J. Zhang, Int. J. Heat Mass Transf. **146**, 118832 (2020)
29. S.M. Hashem Zadeh, S.A.M. Mehryan, M. Ghalambaz, M. Ghodrat, J. Young, A. Chamkha, Energy **213**, 118761 (2020)
30. S.A.M. Mehryan, M. Ghalambaz, L. Sasani Gargari, A. Hajjar, M. Sheremet, J. Energy Storage **28**, 101236 (2020)
31. M.A. Teamah, Int. J. Therm. Sci. **46**, 637 (2007)
32. G.H.R. Kefayati, Energy **107**, 917 (2016)
33. A. Sathiyamoorthi, S. Anbalagan, Chinese J. Phys. **56**, 2155 (2018)
34. S. Arun, A. Satheesh, J. Taiwan Inst. Chem. Eng. **95**, 155 (2019)
35. R. Parveen, T.R. Mahapatra, Heliyon **5**, e02496 (2019)
36. A. M. Aly, Phys. A Stat. Mech. Its Appl. **546**, (2020).
37. M. Ghalambaz, S.M. Hashem Zadeh, S.A.M. Mehryan, I. Pop, D. Wen, Appl. Math. Model. **77**, 1936 (2020)
38. A. Abdulkadhim, A.M. Abed, A.M. Mohsen, K. Al-Farhany, Math. Model. Eng. Probl. **5**, 395 (2018)
39. K. Al-Farhany, A. Abdulkadhim, J. Eng. Appl. Sci. **13**, 6823 (2018)
40. W. Al-Kouz, K.B. Saleem, A. Chamkha, Int. Commun. Heat Mass Transf. **116**, 104719 (2020)
41. K.B. Saleem, W. Al-Kouz, A. Chamkha, Numerical analysis of rarefied gaseous flows in a square partially heated two-sided wavy cavity with internal heat generation. J. Therm. Anal. Calorim. (2020). https://doi.org/10.1007/s10973-020-09959-3
42. R. Nikbakhti, A.B. Rahimi, J. Taiwan Inst. Chem. Eng. **43**, 535 (2012)
43. S.V. Patankar, *Numerical Heat Transfer and Fluid Flow* (Taylor & Francis, Abingdon, 1980).
44. K.B. Saleem, L. Koufi, A.K. Alshara, L. Kolsi, Int. J. Mech. Sci. **181**, 105728 (2020)